ARTICLE

Laser Ablation Atomic Beam Apparatus with Time-Sliced Velocity Map Imaging for Studying State-to-State Metal Reaction Dynamics[†]

Chang-wu Dong[‡], Jia-xing Liu[‡], Fang-fang Li, Feng-yan Wang[*]

Department of Chemistry, Collaborative Innovation Centre of Chemistry for Energy Materials, Fudan University, Shanghai 200433, China

(Dated: Received on December 3, 2015; Accepted on January 4, 2016)

We report a newly constructed laser ablation crossed molecular beam apparatus, equipped with time-sliced velocity map imaging technique, to study state-to-state metal atom reaction dynamics. Supersonic metal atomic beam is generated by laser vaporization of metal rod, and free expansion design without gas flow channel has been employed to obtain a good quality of metal atomic beam. We have chosen the crossed-beam reaction Al+O_2 to test the performance of the new apparatus. Two-rotational-states selected AlO($X^2\Sigma^+$, v=0, N and N+14) products can be imaged via P(N) and R(N+14) branches of the Δv=1 band at the same wavelength, during (1+1) resonance-enhanced multi-photon ionization through the AlO($D^2\Sigma^+$) intermediate state. In our experiment at 244.145 nm for simultaneous transitions of P(15) and R(29) branch, two rings in slice image were clearly distinguishable, corresponding to the AlO(v=0, N=15) and AlO(v=0, N=29) states respectively. The energy difference between the two rotational levels is 403 cm^{-1}. The success of two states resolved in our apparatus suggests a better collisional energy resolution compared with the recent research study [J. Chem. Phys. 140, 214304 (2014)].

Key words: Time-sliced velocity map imaging, Crossed beam, Laser ablation, Metal atom reaction dynamics

I. INTRODUCTION

Studies of collision reaction dynamics of metal atoms in gas phase can provide substantial quantitative and qualitative information on chemical reactivity of metals at atomic and molecular level. Among various experimental techniques, the crossed-beam method has been employed for investigation of single-collision process with one supersonic metal atomic beam [1−3].

The development of metal atomic beams has been for years accompanied with the advances in metal-containing cluster beams [4]. In earlier studies most of research groups have utilized metal-oven effusive sources. In 1981, Smalley and co-workers generated supersonic metal cluster beams with greater intensity by using pulsed laser vaporization method [5]. A similar design was adopted by Costes *et al.* in 1987 for the generation of supersonic metal atomic beam in crossed-beam experiments [1] followed by Davis group [2] and Honma group [3]. Subsequently, in 1999, Costes research group modified the design for metal atomic beam to a "free ablation condition" without gas flow channel [6].

Duncan in 2012 systemically reviewed various designs of laser vaporization [4]. As suggested in Ref.[4], a "cut-away" or "offset" source would be preferred to produce more metal atoms instead of clusters. This design suggests a relatively free expansion condition for gas flow, resulting in negligible formation of large sizes of clusters. The various factors affecting the quality of supersonic atomic beam include carrier gas, backing pressure, temporal duration of the gas pulse, timing of the gas pulse relative to the vaporization laser pulse, laser wavelength, laser pulse energy, focus condition, and the position of metal rod relative to the pulse valve.

In the earlier metal reaction experiments, various detection methods including laser induced fluorescence and quadruple mass spectrometer with electron impact or pulsed photoionization, were employed to obtain the internal energy distributions or translational energy distributions of products [1, 2, 7−11]. By using rotatable beam sources, angular distributions of products can be determined [2].

Recently, time-sliced velocity map imaging technique has been applied in metal atom reaction studies to determine the speed and angular distributions of products [12−14]. As a highly successful method in studying molecular reaction dynamics [15−17], time-sliced velocity map imaging shows a high speed and angular

[†]Part of the special issue for "the Chinese Chemical Society's 14th National Chemical Dynamics Symposium".
[‡]They contributed equally to this work.
[*]Author to whom correspondence should be addressed. E-mail: fengyanwang@fudan.edu.cn

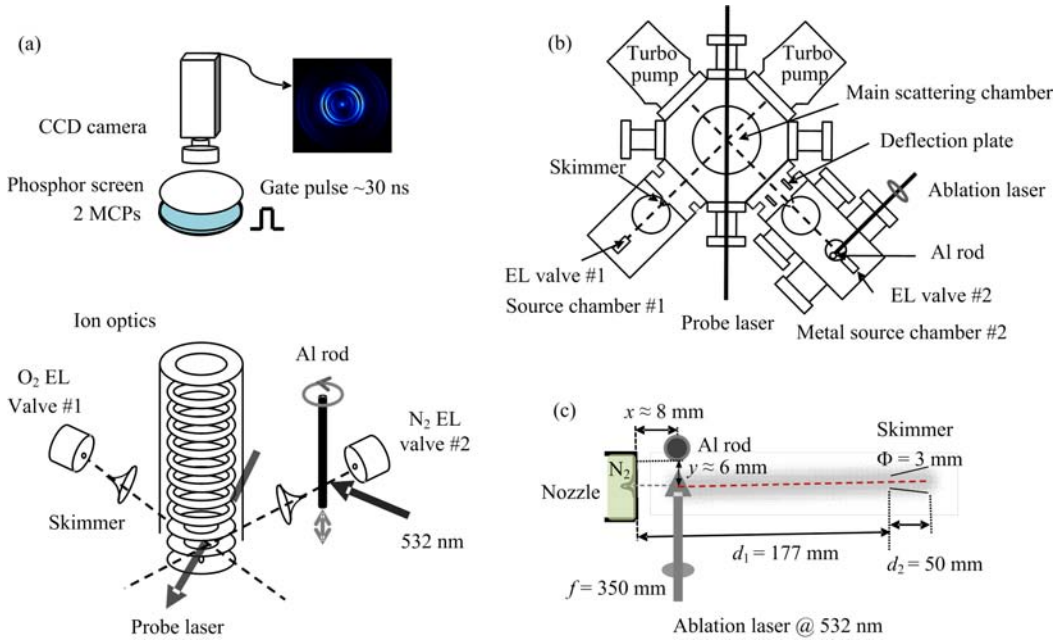

FIG. 1 Schematic view of (a) crossed-beam apparatus for studying metal atomic reaction dynamics, (b) crossed-beam chambers, and (c) supersonic aluminium atomic beam source generated by laser ablation.

resolution. Irrespective of initial positions in crossed-beam defined plane, the reaction products with the same velocity vector will be projected onto one point on the detector. In combination with resonance-enhanced multiphoton ionization (REMPI), the reaction products can be state-selectively studied with time-sliced velocity map imaging.

The experiment of reaction $Al+O_2 \rightarrow AlO+O$ has been carried out to test the performance of new crossed-beam machine. The oxidation dynamics of aluminium atoms has been extensively studied by using Laser-induced fluorescence (LIF) method [1, 3, 6, 7, 9, 18, 19]. Till 2014, time-sliced velocity map imaging method in combination with REMPI has been used to study state-to-state oxidation dynamics of Al atoms [14]. With the same reaction system studied in this report, a better energy resolution has been achieved in comparison with a previous research work [14].

II. APPARATUS

The schematic of the experimental setup for metal atom reaction studies is shown in Fig.1(a). The apparatus basically includes two chambers, for production of two supersonic atomic or molecular beams, and main chamber for reaction and detection system. Briefly, one supersonic metal atomic beam is produced by laser vaporization of metal rod, and intersects with the other supersonic molecular beam in the centre of ion optics. The neutral products thus formed are state-selectively ionized by OPO/OPA laser systems. The product ions with the same velocity were accelerated and projected upwards by ion optics onto the same point on the position sensitive detector. Slice images are finally recorded by applying gate pulse onto the detector.

In the following part first we will show basic designs of crossed-beam studies. Next, we will describe our de sign on a good quality of supersonic metal atomic beam, which is crucial for metal reaction studies. And lastly, we will demonstrate detection systems, including speed calibration of slice image and reaction product detection method.

A. Crossed-beam chambers

As shown in Fig.1(b), two compact source chambers (∼5 L each) are attached to the main chamber at 90° to each other, and separated from the main chamber by skimmers 3 mm orifice (Beam Dynamics Model No.50). Each source chamber is evacuated by a 300 L/s maglev turbo-molecular pump. The background pressure (with beam off) is 4×10^{-8} torr. Typical operating pressure in the source chamber with beam on is 5×10^{-6} torr.

The main chamber has eight side-ports. The intersection angle of two source chambers could be changed to 45° and 135° according to experimental requirements. Two hybrid turbo-molecular pumps (80 L/s) were installed in the main chamber, collinear with two source regions respectively. This arrangement is similar to Jansen *et. al.*'s design [20]. Two maglev turbo-molecular pumps (700 and 300 L/s) were added to the main chamber in reaction and time-of-flight (TOF) regions respectively. The flight distance of ionized products from crossed molecular beam region to the detector

DOI:10.1063/1674-0068/29/cjcp1512261

is 650 mm. Background pressure in the main chamber is 1×10^{-8} torr.

B. Supersonic metal atomic beam

As discussed in the introduction, the "cut away" or "off set" source without gas flow channel, proposed by Duncan [4], provides a good quality supersonic metal atomic beam having more single metal atoms instead of clusters. As shown in Fig.1(c), the supersonic metal atomic beam is produced by using a pulsed supersonic nozzle source for collisional cooling of hot plasma formed by laser ablation. Even-Lavie valves are used for supersonic gas source with a short pulse duration (22−28 μs) and backing pressure ∼15 atm for N_2 carrier gas. The short beam pulse duration indicates only interaction within ∼20 mm relevant to the beam propagation condition. Moreover, Even-Lavie valves with 40° cone of nozzle produce a high on-axis intensity. Even suggested moving the skimmer to larger distance from the nozzle (as large as 150 mm for Ne), in order to allow for a reasonable beam transmission [21]. In our experiments, the optimized separation between the nozzle and the skimmer is 170 mm.

Vaporization design varies with the types of sample studied. Aluminium metal rod (97% Al, Alfa) is used in our studies. The metal rod is controlled by a named *XYZT* multimotion stage, providing a manual actuation of X and Y motions, a stepper motor actuated Z motion (1 μm half step) and an inline-mounted stepper motor for spin motion (step angle 1.8°). Accordingly, the XY position, Z motion and the rotation rate need to be adjusted for optimizing the production of metal atomic beam. The slowest rate (1000 step/min for rotation, 500 step/min for Z motion) is used in our experiment to make the sample last longer. Continuum Minilite II is used for laser ablation with a pulsed width 3−7 ns at the repetition rate of 15 Hz. The laser beam is focused onto the surface of Al rod with a focus lens (f=350 mm). The ablation wavelength 532 nm works much better than 1064 nm. Pulsed energy 6−8 mJ is used for crossed-beam signal accumulation.

As shown in Fig.1(c), the aluminium rod is offset with respect to the carrier supersonic beam. In this design, the metal plume has a chance to spread in space before it encounters the supersonic beam. The supersonic beam must then pick up the metal in the way, and turn it to go in the flying direction of supersonic beam. Even has simulated the collisions of two crossed beams near the nozzle exit, and also suggested the ablated beam few cm from the nozzle (U. Even, personal communication, July, 2015). In our experiment, the metal rod is moved ∼8 mm away from the nozzle and ∼6 mm away from the centre line of expansion direction of supersonic beam.

The Al(^{2}P) atomic beam was detected by (1+1) resonant-enhanced multiphoton ionization (REMPI) via the Al(^{2}D) intermediate state, for Al($^2P_{1/2}$) at 308.305 nm and Al($^2P_{3/2}$) 309.360 nm respectively. The signal of Al(^{2}P) was so strong that the detector would be easily saturated. An unfocused laser with weak pulse energy (<1 mJ) was used for (1+1) REMPI detection. The intensity and speed of Al atoms were obtained by recording velocity mapped images of Al ions. From the recorded Al(^{2}P) spectra, we get a ratio Al($^2P_{3/2}$)/Al($^2P_{1/2}$)=0.12±0.02 (one standard devation for error bar), which agrees with the earlier measurement [14].

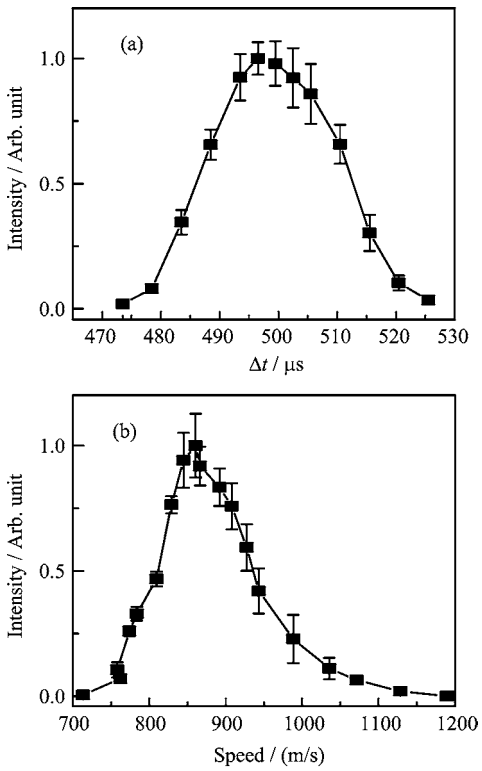

FIG. 2 (a) Intensity of the supersonic Al atomic beam recording via (1+1) resonance-enhanced multiphoton ionization at 308.305 nm as a function of time delay between ablation laser and probe laser. The speed of detected Al atoms is determined by the carrier gas. Δt is determined by probe laser-ablation laser. (b) Speed distribution of supersonic Al atomic beam with peak at 870 m/s. The error bars shown in the figure are ±1000 devation.

Figure 2(a) shows the intensity of supersonic Al atomic beam, detected via (1+1) REMPI at 308.305 nm, as a function of time delay between the ablation laser and the probe laser. The distribution of Al atomic beam indicates a pulse width of ∼20 μs FWHM. The Al beam speed is determined by carrier gas and calibrated by velocity mapping. Figure 2(b) shows the speed distribution of supersonic Al atomic beam with peak at 870 m/s. The speed distribution is obtained by recording the velocity mapped images of Al($^2P_{1/2}$) (speed obtained from velocity mapped image) as a function of time delay between supersonic metal atomic beam (nozzle open timing relative to the vapor-

DOI:10.1063/1674-0068/29/cjcp1512261

ization laser pulse keeps unchanged) and probe laser. The quality of speed distribution is defined by the speed ratio $S=v/\Delta v$. S=8 is obtained from Fig.2(b), a good ratio for the supersonic metal atomic beam. In crossed-beam experiment, only the products staying in the detection region of probe laser (pulse width ∼7 ns) can contribute to the signal accumulation. This suggests the intersection of two beams on the time scales of several microseconds, which is correlated to spot size of probe laser, velocity of two beams and velocity of products. As a result, the speed ratio of the atomic beam for collisions would be much higher than the measured value (∼8).

C. Detection system

Ion optics, comprising of 23 circular electrode plates to perform time-sliced velocity map imaging, is similar to the weak field direct current design described by Lin *et al.* [16]. With the total voltage of 1 kV applied on the ion optics, a weak extraction field ∼2.4 V/mm is held on the first four pieces of stainless steel plates. Then electric field gradually increase to 4.8 V/mm on the next six pieces of plates. The last 13 plates extend 4.8 V/mm for acceleration. The employment of the weak field is to spread the ion turn around time to several hundred nanoseconds, and the transition from weak field to strong field is used to softly focus the ions with the same velocity to the same point on the detector.

Detector is composed of two MCPs (75 mm, 60:1, 10 μm pore, 12 μm pitch, Photek) and one phosphor screen (P43, Photek). Non-gated operation on detector provides the TOF output of multi-mass that pass through the detector. The front MCP is set at 0.9 kV relative to ground and rear MCP is kept at 1.8 kV. Screen is set to 5 kV relative to the rear MCP. In the detector gated configuration, a gate unit works by coupling the 0.5 kV gate pulse onto the rear MCP. Photons emitted by P43 are captured by CCD camera (La Vision E-lite 1.4M). Event counting, an improved counting method for a better imaging resolution [22], is integrated into Davis 8.2 version for data acquisition and accumulation.

Velocity calibration is done by time-sliced velocity map imaging of O^+ ions produced from multiphoton dissociation/ionization of O_2 molecular beam at 224.999 nm [26]. The wavelength is produced by a seeded DICP-made OPO/OPA laser (built in-house at Dalian Institute of Chemical Physics) [23, 24] pumped at 532 nm by a Nd:YAG laser. Laser energy 2 mJ/pulse was used. The gate width on the detector was 30 ns and total voltage applied on the ion optics was 1.8 kV. Figure 3 shows the raw slice image of O^+ ions and corresponding radial distribution (axis label on the top). Assignments of these peaks in the radial distributions have already been done and the kinetic energy data are used for speed calibration [25]. With the speed calibration factor the radial distribution can be transformed to speed distribution (axis label at the bottom). A high speed resolution (∼5%) has been obtained in this apparatus.

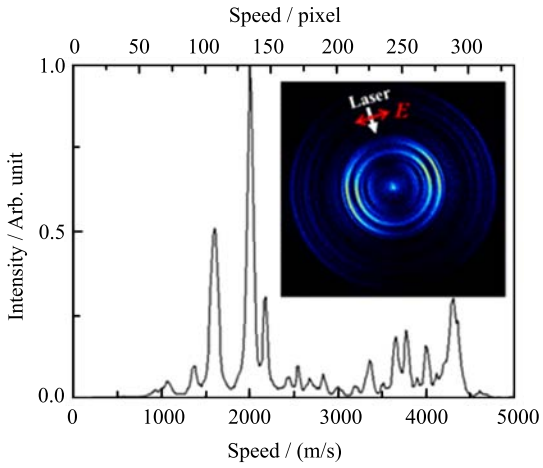

FIG. 3 Raw slice image of O^+ ions produced from multiphoton dissociation/ionization of O_2 molecular beam at 224.999 nm and correspondingly speed distribution of O^+ ions obtained from slice image (pixel shown on the top and m/s at the bottom).

III. STATE-TO-STATE METAL REACTION DYNAMICS

We employed time-sliced velocity map imaging technique for studying the reaction of Al atoms with O_2 molecules at the collisional energy of 2.30 kcal/mol. This is a barrier-less reaction with ΔH=−3.58 kcal/mol. Thus the available energy for products is 5.88 kcal/mol (2057 cm^{-1}). There action cross section decreases with the increase of collisional energy [7−9, 26].

$$Al(^2P_J)+O_2(X^3\Sigma_g^-)\rightarrow AlO(X^2\Sigma^+)+O(^3P_J)$$

In the above reaction, $Al(^2P_{3/2})$ lies 112.061 cm^{-1} higher than $Al(^2P_{1/2})$. The relative reaction cross section, $\sigma(^2P_{3/2})/\sigma(^2P_{1/2})\approx 0.45$, was derived from the previous studies at the collisional energy of 2.3 kcal/mol [6]. Considering $Al(^2P_{3/2})/Al(^2P_{J=1/2,3/2})\approx 0.10$, the reaction of $Al(^2P_{3/2})$ makes a negligible contribution (∼3%) to the width of kinetic energy distributions of $AlO(X^2\Sigma^+, v=0, N)$ products. Populations of the spin-orbit levels of $O(^3P_2)$, $O(^3P_1)$ (158.265 cm^{-1}) and $O(^3P_0)$ (226.977 cm^{-1}) were determined by earlier LIF studies to be 3.8, 1.0, and 0.2 respectively at the collisional energy of 2.9 kcal/mol [19]. Thus the width of kinetic energy distributions of $AlO(X^2\Sigma^+, v=0, N)$ products is mainly related to the width of the collisional energy and the populations of two spin-orbit levels of counter products, $O(^3P_{J=2,1})$.

For studies of Al+O_2 reaction, the AlO products were

DOI:10.1063/1674-0068/29/cjcp1512261

detected by (1+1) REMPI via $D^2\Sigma^+$-$X^2\Sigma^+$ transition in the wavelength region of 243−245 nm. Slice images of two-rotational-states selected AlO($X^2\Sigma^+$, v=0, N and N+14) products can be recorded via P(N) and R(N+14) branches of the Δv=1 band at the same wavelength. The laser beam is generated from a continuum's sunlite OPO/OPA laser pumped at 355 nm by a second Nd:YAG laser. Pulse width of the laser is ∼7 ns. Pulse energy 1−3 mJ was used with cylindrical lens f=500 mm. Probe laser has a large spot ∼6 mm. The AlO background in the Al atomic beam was gradually decreased with time as oxide contamination on the surface of Al rod being etched out by laser ablation.

Figure 4 shows the raw image of AlO products recorded at 244.145 nm with two clear rings. The AlO beam background has been subtracted and traces of little amount of residual background could be found in the Al beam expanding direction. At 244.145 nm both transitions of P(15) and R(29) branches were probed. The outer ring with fast speed corresponds to AlO(N=15) and inner ring with slow speed to AlO(N=29). The energy difference between the two rotational states is 403 cm^{-1}. This suggests a narrower width of the collisional energy than 403 cm^{-1}. The success of the separation of the two rings in our apparatus suggests a better collisional energy distribution compared with the previous experimental studies on the reaction of Al atoms with O_2 molecules [14].

Newton diagram is shown in Fig.4. The angular distributions of AlO products show a backward and forward peaking for the two rotational states of AlO(v=0, N=15 and 29) products. As the product rotational level N increases from 15 to 29, more products have been distributed to side way scattering.

As rotational level N increases, the energy difference between the two rotational states AlO(N and N+14) will be increased. This suggests that two rings corresponding to the two rotational states will be separated more clearly. With the high resolution of slice ion imaging and narrow width of collisional energy distribution in crossed beam apparatus, the velocity distributions and angular distributions of state specific AlO products would be discussed in more detail in the future work.

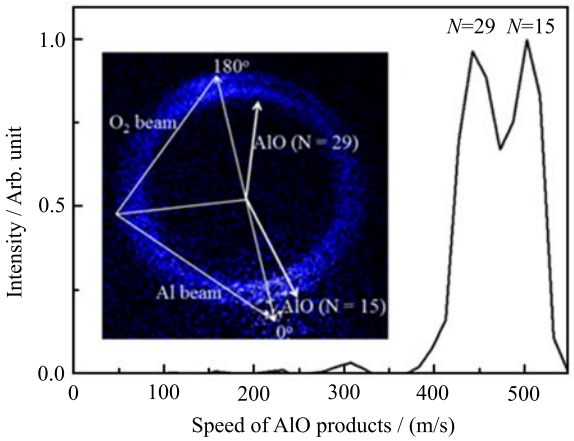

FIG. 4 Raw slice image of two-rotational-states selected AlO(X, v=0, N=15 and 29) products from the crossed-beam reaction of Al+O_2 at the collisional energy of 2.3 kcal/mol and speed distribution of AlO products obtained from the slice image. The AlO products were detected by (1+1) resonance-enhanced multi-photon ionization via P(15) and R(29) transition at the same wavelength of 244.145 nm. The speed distribution is obtained by integration of strong signal shown in the forward scattering in the angular range of ±20°. Two rings were clearly distinguished: inner ring with low speed corresponding to AlO(v=0, N=29) and outer ring with fast speed to AlO(v=0, N=15). The energy difference between the two rotational states is 403 cm^{-1}. Newton diagram is shown in the figure. Small traces of AlO background from single beam can be found in the Al beam expanding direction.

IV. CONCLUSION

We have constructed a new crossed-beam apparatus for studying state-to-state metal atom reaction dynamics. Supersonic metal atomic beam has been generated by laser vaporization of metal rod in free expansion design without gas flow channel. Variable key factors have been optimized for generation of a good quality of supersonic aluminium atomic beam. Crossed-beam reaction Al+O_2→AlO+O has been studied to test the performance of the new apparatus. Two-rotational-states selected AlO($X^2\Sigma^+$, v=0) reaction products were imaged via P(15) and R(29) branch of the Δv=1 band at 244.145 nm, by (1+1) resonance-enhanced multiphoton ionization through the AlO($D^2\Sigma^+$) intermediate state. The energy difference between the AlO(v=0, N=15) and AlO(v=0, N=29) states is 403 cm^{-1}. The success of two rings separation in our experiment suggests a good collisional energy resolution for further crossed-beam studies.

V. ACKNOWLEDGMENTS

We are indebted to Prof. Kopin Liu (IAMS, Taipei) for stimulating discussions on going experiments, to Prof. Ming-fei Zhou and Assoc. Prof. Guan-jun Wang (Fudan University, Shanghai) for assistance in building machine, to Prof. Uzi. Even (Tel Aviv University, Tel Aviv) for discussions on El valve employment in laser ablation, and to Prof. Xue-ming Yang's group (DICP, Dalian) for new laser system. This work was supported by the National Natural Science Foundation of China (No.21322309) and the Program for Professor of Special Appointment (Eastern Scholar) at Shanghai Institutions of Higher Learning.

DOI:10.1063/1674-0068/29/cjcp1512261

[1] M. Costes, C. Naulin, G. Dorthe, C. Vaucamps, and G. Nouchi, Faraday Discuss. **84**, 75 (1987).
[2] P. A. Willis, H. U. Stauffer, R. Z. Hinrichs, and H. F. Davis, Rev. Sci. Instrum. **70**, 2606 (1999).
[3] K. Honma, J. Chem. Phys. **119**, 3641 (2003).
[4] M. A. Duncan, Rev. Sci. Instrum. **83**, 041101 (2012).
[5] T. G. Dietz, M. A. Duncan, D. E. Powers, and R. E. Smalley, J. Chem. Phys. **74**, 6511 (1981).
[6] C. Naulin and M. Costes, Chem. Phys. Lett. **310**, 231 (1999).
[7] P. J. Dagdigian, H. W. Cruse, and R. N. Zare, J. Chem. Phys. **62**, 1824 (1975).
[8] L. Pasternack and P. J. Dagdigian, J. Chem. Phys. **67**, 3854 (1977).
[9] K. M. Chen, C. H. Sung, J. L. Chang, T. H. Chung, and K. H. Lee, Chem. Phys. Lett. **240**, 17 (1995).
[10] K. Liu and J. M. Parson, J. Chem. Phys. **67**, 1814 (1977).
[11] H. W. Cruse, P. J. Dagdigia, and R. N. Zare, Faraday Discuss. **55**, 277 (1973).
[12] K. Honma and Y. Matsumoto, Phys. Chem. Chem. Phys. **13**, 8236 (2011).
[13] K. Honma and Y. Matsumoto, J. Chem. Phys. **136**, 034301 (2012).
[14] K. Honma, K. Miyashita, and Y. Matsumoto, J. Chem. Phys. **140**, 214304 (2014).
[15] C. R. Gebhardt, T. P. Rakitzis, P. C. Samartzis, V. Ladopoulos, and T. N. Kitsopoulos, Rev. Sci. Instrum. **72**, 3848 (2001).
[16] J. J. Lin, J. Zhou, W. Shiu, and K. Liu, Rev. Sci. Instrum. **74**, 2495 (2003).
[17] M. N. Ashfold, N. H. Nahler, A. J. Orr-Ewing, O. P. Vieuxmaire, R. L. Toomes, T. N. Kitsopoulos, I. A. Garcia, D. A. Chestakov, S. M. Wu, and D. H. Parker, Phys. Chem. Chem. Phys. **8**, 26 (2006).
[18] C. Naulin and M. Costes, J. Phys. Chem. **98**, 5593 (1994).
[19] M. Ishida, T. Higashiyama, Y. Matsumoto, and K. Honma, J. Chem. Phys. **122**, 204312 (2005).
[20] P. Jansen, D. W. Chandler, and K. E. Strecker, Rev. Sci. Instrum. **80**, 083105 (2009).
[21] U. Even, Adv. Chem. **2014**, 1 (2014).
[22] B. Y. Chang, R. C. Hoetzlein, J. A. Mueller, J. D. Geiser, and P. L. Houston, Rev. Sci. Instrum. **69**, 1665 (1998).
[23] T. Wang, J. Chen, T. Yang, C. Xiao, Z. Sun, L. Huang, D. Dai, X. Yang, and D. H. Zhang, Science **342**, 1499 (2013).
[24] T. Wang, T. Yang, C. Xiao, D. Dai, and X. Yang, J. Phys. Chem. Lett. **4**, 368 (2013).
[25] A. T. J. B. Eppink and D. H. Parker, Rev. Sci. Instrum. **68**, 3477 (1997).
[26] S. D. Le Picard, A. Canosa, D. Travers, D. Chastaing, B. R. Rowe, and T. Stoecklin, J. Phys. Chem. A **101**, 9988 (1997).

DOI:10.1063/1674-0068/29/cjcp1512261